J Mol Model (2009) 15:1043–1049
DOI 10.1007/s00894-009-0457-6

ORIGINAL PAPER

Theoretical study on the thermal decomposition of model compounds for Poly (dialkyl fumarate)

Yanling Wang · Xueye Wang · Liming Liu · Xinyu Peng

Received: 6 November 2008 / Accepted: 6 January 2009 / Published online: 11 February 2009

Abstract The thermal decomposition of model compounds for poly (dialkyl fumarate) was studied by using *ab initio* and density functional theory (DFT) calculations. To determine the most favorable reaction pathway of thermal decomposition, geometries, structures, and energies were evaluated for reactants, products, and transition states of the proposed pathways at the HF/6-31G(d) and B3LYP/6-31G (d) levels. Three possible paths (I, II and III) and subsequent reaction paths (IV and V) for the model compounds of poly (dialkyl fumarate) decomposition had been postulated. It has been found that the path (I) has the lowest activation energy 193.8 kJ mol^{-1} at B3LYP/6-31G (d) level and the path (I) is considered as the main path for the thermal decomposition of model compounds for poly (dialkyl fumarate).

Keywords Density functional theory (DFT) · Diethyl succinate · Poly (dialkyl fumarate) · Thermal decomposition mechanism

Introduction

Poly (dialkyl fumarate) is shown to have properties of interest for engineering applications. Diethyl fumarate was recently investigated to be used as biodegradable polymers for the treatment of large bone defects [1–3]. The thermal decomposition of poly (di-itaconates), polymethacrylates and polyacrylates have been studied to a considerable extent [4–11]. However, the thermal decomposition of poly (dialkyl fumarates) has only rarely been studied. There was only one detailed study [3] of the decomposition of dialkyl fumarate monomers and several, but not detailed, investigations of the polymers [12, 13]. Hence, the goal of this study was to attempt to determine the mechanism of the thermal decomposition behavior of poly (dialkyl fumarate) and the most favorable reaction pathway of thermal decomposition.

In this paper, we cite the model compounds for representing structural units of poly (dialkyl fumarate) [14]. There is substantial evidence that one or more of the following pathways (I [15], II and III [15]) and subsequent pathways (IV and V) [15] take place during the thermal decomposition of model compounds (Scheme 1).

Y. Wang · X. Wang (✉) · L. Liu · X. Peng
College of Chemistry, Key Laboratory of Materials Design and Preparation Technology of Hunan Province,
Xiangtan University,
Xiangtan,
Hunan 411105, People's Republic of China
e-mail: wxueye@xtu.edu.cn

Computational methods

The geometries of reactants, products, and transition states (TSs) were fully optimized by the energy gradient methods. All optimized geometries were obtained by using the HF and the Becke 3LYP (B3LYP) [16, 17] hybrid density functional with the 6-31G(d) basis set. Vibrational frequencies were calculated at all stationary points to obtain zero-point energies (ZPE) and thermodynamic parameters at the HF/6-31G(d) and B3LYP/6-31G(d) levels. At the B3LYP/6-31G(d) level the intrinsic reaction coordinate (IRC) [18–20] was carried out for each transition state to make sure that it is the transition structure connecting the desired reactants and products. All calculations were carried out with the Gaussian 03 program [21].

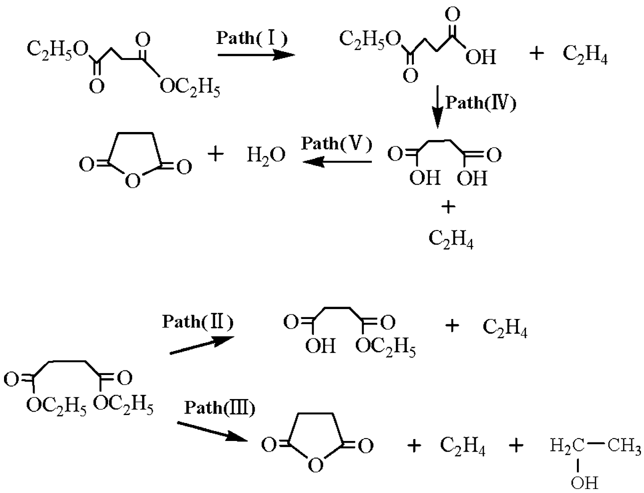

Scheme 1 Possible reaction pathways for the model compound of poly (dialkyl fumarates)

Results and discussion

The thermal decomposition of the model compounds for poly (dialkyl fumarate) was theoretically investigated at 493.15K. Table 1 gives the thermal parameters of the three possible decomposition processes. There is no experimental data for the structures of all reactants, products and transition states. The HF bond lengths, bond angles and dihedral angles are compared with the B3LYP results. Figure 1 shows the optimized geometry of model compounds *s*-(E) - diethyl succinate (**R1**) and *s*-(Z) - diethyl succinate (**R2**) for poly (dialkyl fumarate) and some other reactants. The optimized structures of the decomposition products are shown in Fig. 2, while the optimized various transition states structures (TSs) are presented in Fig. 3. Figure 4 shows the IRC for the paths (I, II, III, IV and V) transform process.

Reaction path (I)

As shown in Scheme 1, Figs. 1, 2, 3 and Table 1, path (I) is an elimination reaction with formation of **P1**, which proceeds through a six-centered-ring transition state **TS1** with ΔG=43.1 kJ mol^{-1} and ΔH=72.0 kJ mol^{-1} at the B3LYP/6-31G(d) level of theory. The thermal enthalpy of this reaction path is 65.3 kJ mol^{-1} at the HF/6-31G(d) level of theory. The free energy of this reaction path is 29.7 kJ mol^{-1} at the HF/6-31G(d) level of theory. The activation energy of path (I) is 193.8 kJ mol^{-1} at the B3LYP/6-31G(d) level of theory, which is 67.1 kJ mol^{-1} higher in energy than the HF/6-31G(d) energy of theory. Figure 4 path (I) shows changes of energy along with reaction coordinate in path (I), and the result verifies that the **TS1** is relative with corresponding reactants and products. The B3LYP-predicted geometry parameters were discussed in this process. Ethylene elimination involves breaking of both C8-H21 and C7-O26 bonds. The breaking C8-H21 and C7-O26 bonds are 1.335 Å and 2.027 Å in **TS1**, respectively. The bond length of C6-C26 changes from 1.265 Å in the **R1** to 1.354 Å in **TS1**. The bond length of C6-C25 is 0.067 Å shorter in **R1** than this in **TS1**. The bond length of C7-C8 changes from 1.521 Å in **R1** to 1.402 Å in **TS1**.

The pathway continues with the β-hydrogen atoms scission in the first step. There are two steps in the subsequent decomposition path (IV) and path (V). The path (IV) involves the breakage of β-bond and formation of a transition state TS4. The energy invested in the cleavage of the second β-bond is ΔG=79.9 kJ mol^{-1} and ΔH= 103.1 kJ mol^{-1} at the B3LYP/6-31G(d) level of theory. The thermal enthalpy and free energy of this reaction path are 102.4 and 70.3 kJ mol^{-1} at the HF/6-31G(d) level of theory. And the activation energy for the second ethylene is 273.0 kJ mol^{-1} at the B3LYP/6-31G(d) level of theory, which is 46.8 kJ mol^{-1} lower in energy than the HF/6-31G (d) energy of theory. For TS4 of the path (IV), intrinsic

Table 1 Calculated thermodynamic parameters for the three competitive decomposition processes of model compounds

		ΔG (kJ mol^{-1})	ΔH (kJ mol^{-1})	E (kJ mol^{-1})
Path (I)	HF/6-31G(d)	29.7	65.3	260.9
	B3LYP/6-31G(d)	43.1	72.0	193.8
Path (II)	HF/6-31G(d)	36.5	71.3	318.2
	B3LYP/6-31G(d)	47.7	77.2	269.7
Path (III)	HF/6-31G(d)	73.9	122.7	409.7
	B3LYP/6-31G(d)	98.5	120.1	321.3
Path (IV)	HF/6-31G(d)	70.3	102.4	319.8
	B3LYP/6-31G(d)	79.9	103.1	273.0
Path (V)	HF/6-31G(d)	27.5	46.9	256.5
	B3LYP/6-31G(d)	28.7	42.2	194.4

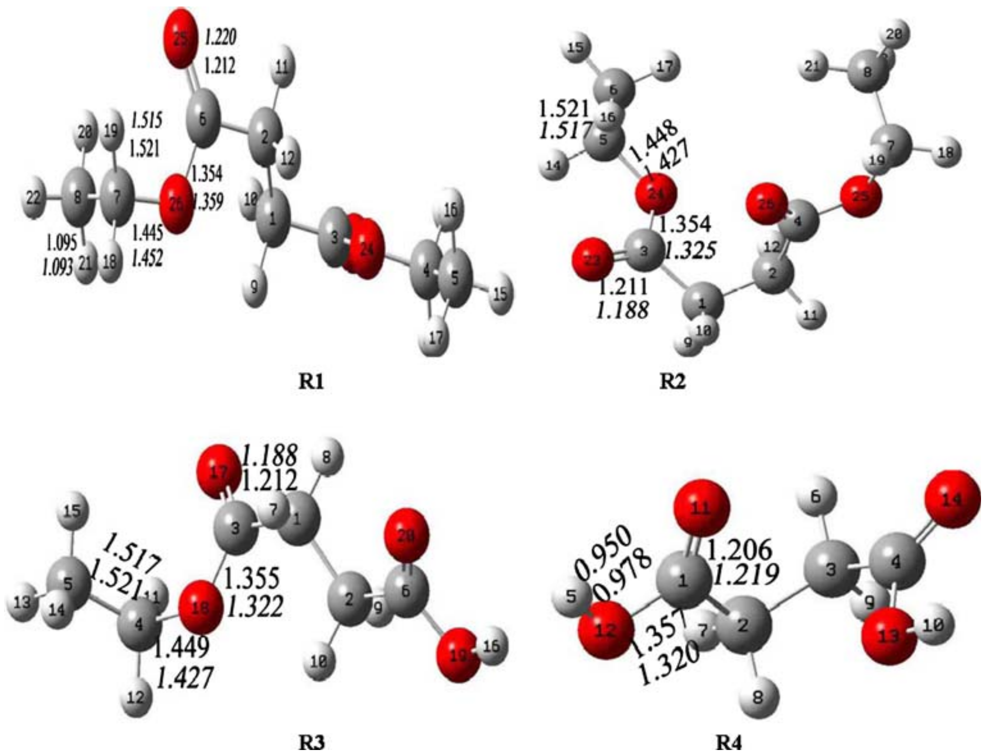

Fig. 1 B3LYP/6-31G(d) optimized geometries for all the reactants. The values in italic fonts are the HF/6-31G(d) results. Distances are in angstroms, and angles are degrees

reaction coordinate (IRC) calculation was carried out upon computation from the unique imaginary vibration mode of TS4 to reactants and products. This shows that the transition state is relative with corresponding reactants and products (Fig. 4). The B3LYP-predicted geometry parameters were discussed in this process. The bond lengths of C3-O18 and C4-C5 shorten from 1.355 Å and 1.521 Å in **R3** to 1.330 Å and 1.395 Å in **TS4**, respectively. The bond length of C3-O17 changes from 1.212 Å in **R3** to 1.223 Å in **TS4**. The distance between O25 and H21 shortens from 3.952 Å in **R3** to 1.002 Å in **TS4**. The breaking C4-O18 and C5-H14 bonds in **TS4** are 2.197 Å and 1.321 Å, respectively. The bond angle of C4-C18-C3 is 2.033° shorter in TS4 than this in **R3**.

According to the calculations two neighboring ester groups loose ethylene by the above mechanism, then maleic anhydride moieties could be formed in the second step path (V). Path (V) is an elimination reaction with formation of **P5** *via* a four-centered transition state **TS5** with ΔG= 28.7 kJ mol^{-1} and ΔH=42.2 kJ mol^{-1} at the B3LYP/6-31G (d) level of theory. The thermal enthalpy and free energy of this reaction path are 46.9 and 27.5 kJ mol^{-1} at the HF/6-31G(d) level of theory. For H_2O elimination is predicted to have activation energy 194.4 kJ mol^{-1} at the B3LYP/6-31G (d) level of theory, and the activation energy of the path is 256.5 at the HF/6-31G(d) level of theory. Figure 4 shows the IRC for the path (V). The B3LYP-predicted geometry parameters were discussed in this process. The dihedral angle of H10-O13-C1-O12 is 0.6° in **TS5**. The breaking H10-O13 and C1-O12 bonds in **TS5** are 1.382 Å and 1.728 Å, respectively. The C4-O13 bond shortens from 1.359 Å in **R4** to 1.328 Å in **TS5**.

Reaction path (II)

From Scheme 1, Figs. 1, 2, 3 and Table 1, it can be seen that path (II) is an elimination of ethylene from **R2** *via* a transition state **TS2**. Ethylene is removed from **R2** with ΔG=47.7 kJ mol^{-1} and ΔH=77.2 kJ mol^{-1} at the B3LYP/6-31G(d) level of theory. The ΔG and ΔH of this reaction path are 36.5 and 71.3 kJ mol^{-1} at the HF/6-31G(d) level of theory. The activation energy of path (II) is 269.7 kJ mol^{-1}, which is 48.5 kJ mol^{-1} lower in energy than the HF/6-31G (d) energy of theory. IRC for this channel shows that the transition state is relative with corresponding reactants and products (Fig. 4). In reaction path (II), the B3LYP-predicted geometry parameters were discussed. The breaking C6-H17 and C5-O24 bonds are 1.300 Å and 2.240 Å in **TS2**, respectively. The bond lengths of C5-C6 and C3-C24 change from 1.521 Å and 1.354 Å in **R2** to 1.392 Å and 1.321 Å in **TS2**, respectively. The bond length of C3-O23 is 0.016 Å longer in **R2** than in **TS2**. The H17-O24 distance shortens from 2.698 Å in **R2** to 1.424 Å in **TS2**. The bond angle of C1-C3-O24 is 4.2° smaller in **R2** than in **TS2**.

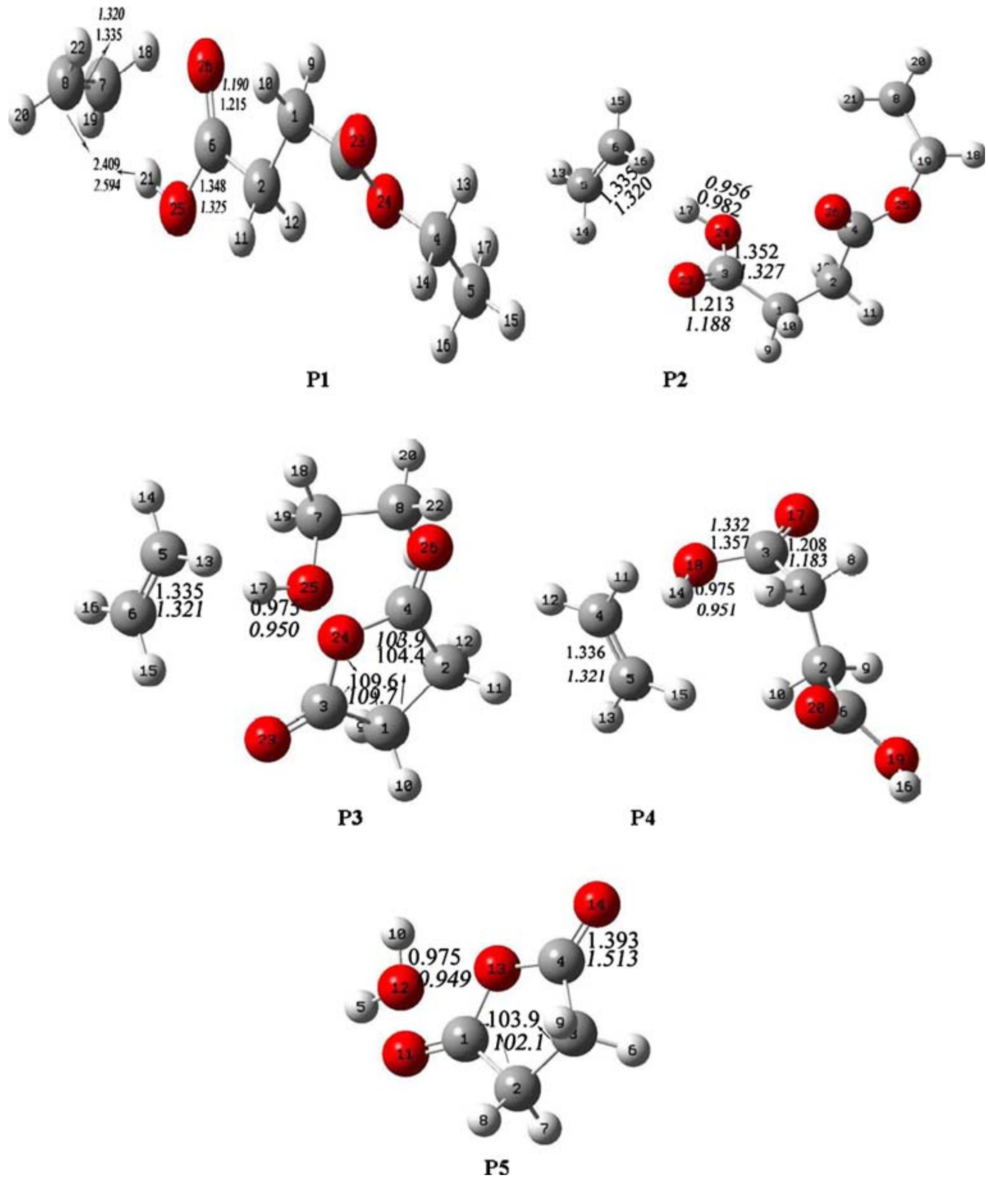

Fig. 2 B3LYP/6-31G(d) optimized geometries for all the products. The values in italic fonts are the HF/6-31G(d) results. Distances are in angstroms, and angles are degrees

Reaction path (III)

Scheme 1, Figs. 1, 2, 3 and Table 1 show that the ethanol eliminates *via* a six-centered transition state **TS3** with C_1 symmetry in the path (III). Afterwards, ethanol, ethylene and maleic anhydride moieties are formed. **P3** is formed with ΔG=98.5 kJ mol^{-1} and ΔH=120.1 kJ mol^{-1} at the B3LYP/6-31G(d) level of theory. The ΔG and ΔH of this reaction path are 73.9 and 122.7 kJ mol^{-1} at the HF/6-31G (d) level of theory. The activation energy of path (III) is predicted to be 321.3 kJ mol^{-1} at the B3LYP/6-31G(d) level of theory, which is 88.4 kJ mol^{-1} lower in energy than the HF/6-31G(d) energy of theory. Figure 4 shows the IRC for path (III). The result shows that the transition state is relative with corresponding reactants and products. In reaction path (III), the B3LYP-predicted geometry parameters were discussed. The breaking C4-O25, C6-H17 and C5-O24 bonds are 1.530 Å, 1.472 Å, and 2.241 Å in **TS3**, respectively. The bond length of C5-C6 changes from 1.521 Å in **R2** to 1.377 Å in **TS3**. The bond length of C3-C24 is 0.049 Å longer in **TS3** than in **R2**. The bond length of C3-C23 is 0.017 Å longer in **TS3** than in **R2**. The bond angle of C2-C1-C3 is 9.6° smaller in **TS3** than in **R2**.

From the discussion above, as to energy of the thermal decomposition of model compounds for poly (dialkyl fumarate), the B3LYP/6-31G(d) results were better than the HF/6-31G(d). The HF/6-31G(d) level of calculations may be insufficient. The DFT level calculations give much

Fig. 3 B3LYP/6-31G(d) optimized geometries for all the transition states. The values in italic fonts are the HF/6-31G(d) results. Distances are in angstroms, and angles are degrees

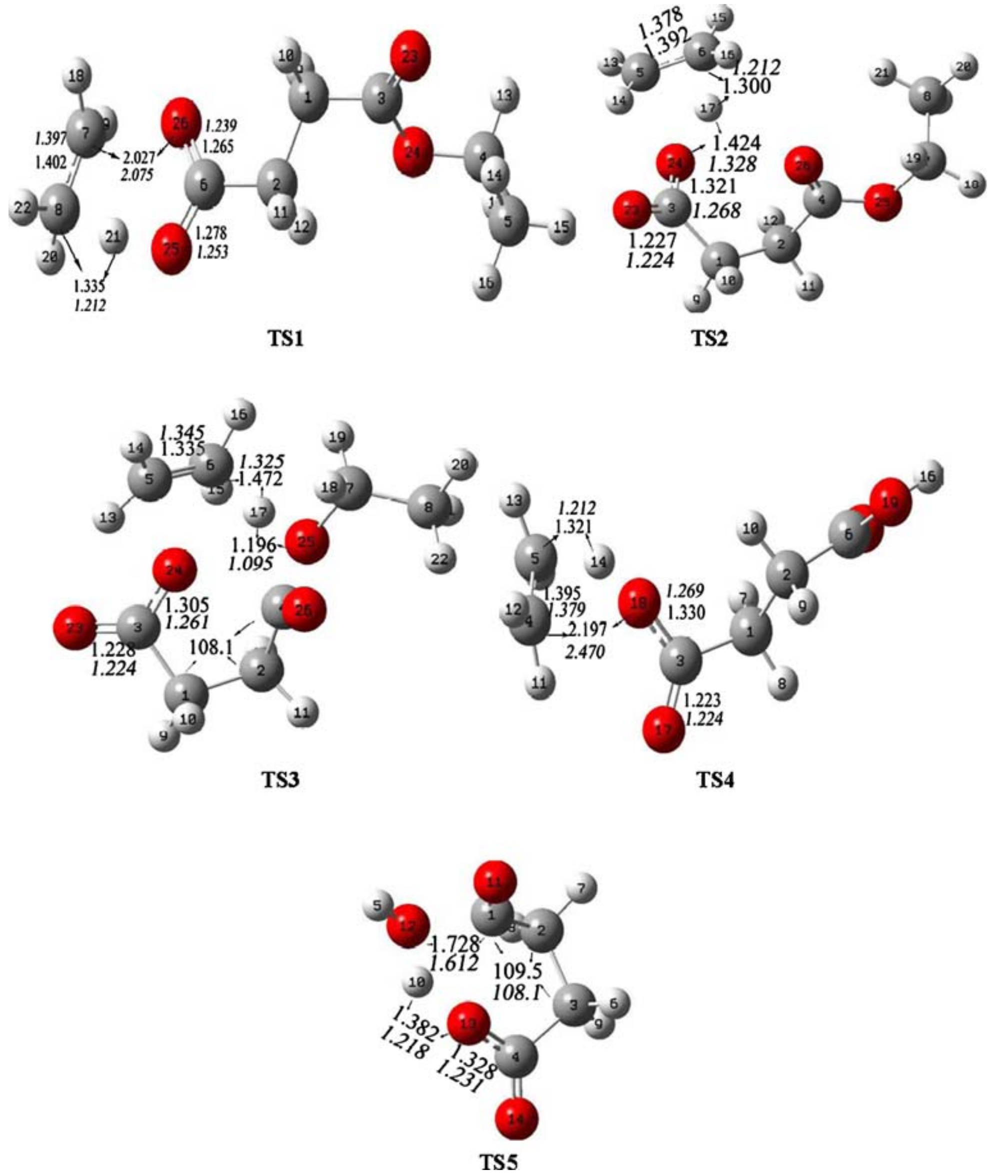

better agreement with the experimental results. According to the B3LYP energies the descending order of energies is path (III) > path (II) > path (I) for the three paths. The energy of path (I) is the lowest which is the most favorable pathway. All of the initial reaction pathways are endergonic. These computed channels are in excellent agreement with the experimental channels [15].

Conclusions

In conclusion, a computational study is conducted for the thermal decomposition of the model compounds to elucidate the thermal decomposition mechanism of the model compounds for poly (dialkyl fumarate). On the basis of the experimental observations, three possible initial pathways have been postulated for model compounds decomposition, and were calculated at 493.15 K. The paths (I, II and III) can take place at lower temperature. However, the calculations suggest that the consecutive ethylene elimination to form maleic anhydride moieties and two molecules ethylene is identified as the energetically most favorable decomposition pathway. The results appear to correlate closely with the experimental channels [15].

Acknowledgements The authors wish to acknowledge the financial supports from the Open Project Program of Key Laboratory of Materials Design and Preparation Technology of Hunan Province, China (KF0802).

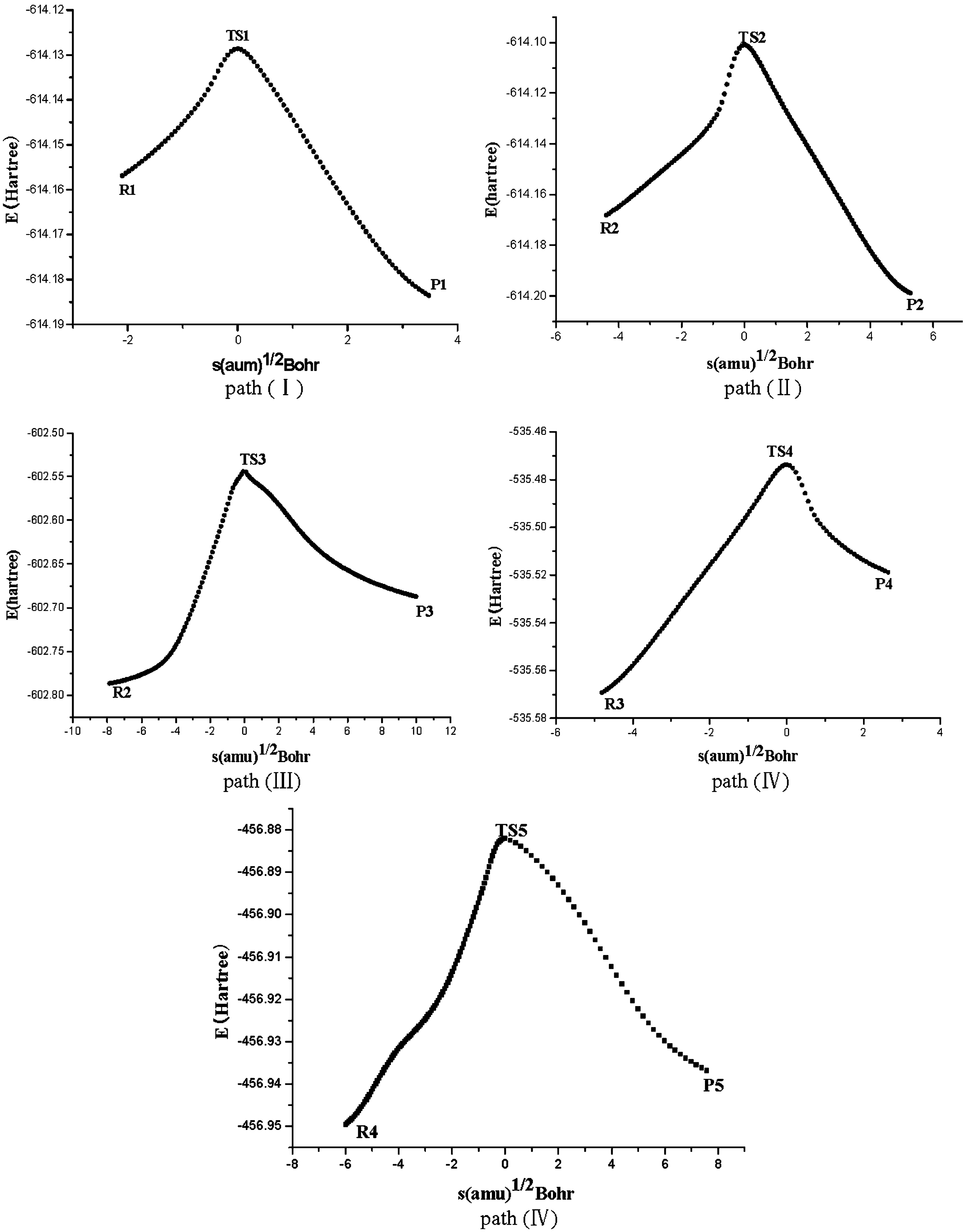

Fig. 4 IRC for paths (I, II, III, IV and V) at the B3LYP/6-31G(d) level

References

1. Burag KJL, Porter S, Kelam JF (2000) Biomaterials 11:2347–2359
2. Suggs LJ, West JL, Mikos AG (1999) Biomaterials 20:683–690
3. Fisher JP, Dean D, Mikos AG (2002) Biomaterials 23:4333–4343
4. Cowie JMG, Haq ZBr (1977) Polym J 9:241–245
5. Popović IG, Katsikas L, Velicković JS (1992) J Therm Anal 38:953–959
6. Popović IG, Katsikas L, Velicković JS (2005) Polym Degrad Stab 89:153–164
7. Popović IG, Katsikas L, Velicković JS (2005) Polym Degrad Stab 89:165–174
8. Grassie N (1972) Pure Appl Chem 30:119–134
9. Grassie N, Scott G (1985) Polymer degradation and stabilization. Cambridge University Press, Cambridge, pp 1–67
10. David C (1975) Thermal degradation of polymers. In: Bamford CH, Tipper CFH (eds) Comprehensive chemical kinetics, vol. 14. Elsevier, Amsterdam, pp 1–174
11. McNeill IC (1989) Thermal degradation. In: Allen G, Bevington JC, Eastmond GC, Ledwith A, Russo S, Sigwalt P (eds) Comprehensive polymer science, vol. 6. Pergamon Press, Oxford, pp 451–500
12. Otsu T, Minai H, Toyoda N, Yasuhara T (1985) Makromol Chem 12S:133–142
13. Otsu T, Yoshioka M, Sunagawa TJ (1992) Polym Sci Part A: Polym Chem 30:1347–1354
14. Tvaroska I, Bleha T, Valko L (1975) Polym J 7:34–43
15. Milovanović M, Bošković R, Tošić T, Katsikas L, Popović IG (2006) Polym Degrad Stab 91:3221–3229
16. Stevens PJ, Devlin FJ, Chabalowski CF, Frisch MJ (1994) J Phys Chem 98:11623–11627
17. Dubnikova F, Kosloff R, Almog J, Zeiri Y, Boese R, Itzhaky H, Alt A, Keinan E (2005) J Am Chem Soc 127:1146–1159
18. Gordon MH, Pople JA (1988) J Chem Phys 89:5777–5786
19. Merino P, Tejero T, Chiacchio U, Romeo G, Rescifina A (2007) Tetrahedron 63:1448–1458
20. Grant DM, Grassie N (1960) Polymer 1:445–455
21. Frisch MJ, Trucks GW, Schlegel HB, Scuseria GE, Robb MA, Cheeseman JR, Zakrzewski VG, Montgomery JA Jr, Stratmann RE, Burant JC, Dapprich S, Millam JM, Daniels AD, Kudin KN, Strain MC, Farkas O, Tomasi J, Barone V, Cossi M, Cammi R, Mennucci B, Pomelli C, Adamo C, Clifford S, Ochterski J, Petersson GA, Ayala PY, Cui Q, Morokuma K, Malick DK, Rabuck AD, Raghavachari K, Foresman JB, Cioslowski J, Ortiz JV, Stefanov BB, Liu G, Liashenko A, Piskorz P, Komaromi I, Gomperts R, Martin RL, Fox DJ, Keith T, Al-Laham MA, Peng CY, Nanayakkara A, Gonzalez C, Challacombe M, Gill PMW, Johnson BG, Chen W, Wong MW, Andres JL, Head-Gordon M, Replogle ES, Pople JA (2003) Gaussian 2003 revision B.05. Gaussian Inc, Pittsburgh, PA